Comparison of different fidelity aerodynamic solvers on the IEA 10 MW turbine including novel tip extension geometries

Behrens de Luna, R.; Marten, D.; Barlas, T.; Horcas, S. G.; Ramos-García, N.; Li, A.; Paschereit, C. O.

Published in:
Turbine Technology; Artificial Intelligence, Control and Monitoring

Link to article, DOI:
10.1088/1742-6596/2265/3/032002

Publication date:
2022

Document Version
Publisher's PDF, also known as Version of record

Comparison of different fidelity aerodynamic solvers on the IEA 10 MW turbine including novel tip extension geometries

Comparison of different fidelity aerodynamic solvers on the IEA 10 MW turbine including novel tip extension geometries

R Behrens de Luna[1], D Marten[1], T Barlas[2], S G Horcas[2], N Ramos-García[2], A Li[2] and C O Paschereit[1]

[1] Chair of Fluid Dynamics, Hermann Föttinger Institute, Technische Universität Berlin, Müller-Breslau-Straße 8, 10623 Berlin, Germany.
[2] Department of Wind Energy, Technical University of Denmark, Frederiksborgvej 399, 4000 Roskilde, Denmark.

E-mail: r.behrensdeluna@tu-berlin.de

Abstract. Lifting-line based solvers could supersede the blade element momentum (BEM) method as the industry standard in the near future as rotor sizes of modern wind turbines and computational resources continue to increase. A comparison study between both methods is presented where the IEA 10 MW wind turbine is evaluated in the aero-servo-elastic simulation tool QBlade, comparing the lifting-line free vortex wake method to an unsteady blade element momentum solver. Besides the baseline rotor of the IEA 10 MW turbine, the comparison includes several blade tip extensions, including a swept and a dihedral geometry, to further differentiate capabilities between both methods in aerodynamically complex flow fields. As a reference serve results from equivalent simulations performed with multiple fidelity solvers of the simulation tool HAWC2. Results of a rigid load case demonstrate considerable improvement regarding the aerodynamic accuracy of lifting-line based methods in below rated conditions over BEM codes. The aerodynamic loads on geometrically complex tip extensions in steady conditions prove good capabilities of lower fidelity codes to predict out-of-plane bend shapes but also clear limitations regarding loads on swept geometries. A quasi-steady aeroelastic load case further demonstrates the capability of both QBlade codes to produce comparable results to similar fidelity solvers of the HAWC2 tool on an integral level. A detailed comparison in the time domain shows a larger dependency of the results on the type of structural solver that is used in contrast to the fidelity level of the aerodynamic method.

1. Introduction

The goal to reduce the levelized cost of energy (LCOE) combined with a growing focus on offshore wind leads to a shift to ever larger wind turbines [1]. Alongside numerous advantages of these modern wind turbine designs, their long, slender and flexible blades increase the complexity of the system considerably. Their blades may undergo large out-of-plane deflections during operation [2] and therefore violate one of the key assumptions of the commonly used blade element momentum (BEM) method, where the momentum balance is carried out in the rotor plane [3]. Computationally more demanding aerodynamic methods, such as the medium fidelity lifting-line (LL) or the high fidelity Navier-Stokes computational fluid dynamics (CFD) methods, promise to increase the accuracy of the predicted aerodynamic loads on such turbines, due to

the ability to resolve the three dimensional blade geometry [2]. Additionally, unlike the BEM method, these higher fidelity solvers are able to resolve the flow around the aerodynamically complex root and tip regions directly without the need for correction models. This capability should increase the accuracy of aeroelastic simulations and allow to evaluate the performance and feasibility of complex tip designs, which are designed to increase the energy output. An aeroelastic model of the IEA 10 MW turbine is set up in the wind turbine simulation tool QBlade [4, 5] in accordance with a model that initially is set up by the wind energy group from the Technical University of Denmark (DTU) in the simulation tool HAWC2 [6]. Two load cases are simulated with QBlade's lifting-line free vortex wake (QLLT [4]) and its recently implemented unsteady polar-BEM method (QBEM). In the second case, structural dynamics are included. The results are compared to the findings obtained by the DTU group using multiple fidelity solvers. Results of the following four HAWC2 solvers serve as references: EllipSys3D (CFD [7]), lifting-line free wake (MIRAS [8]), coupled near- and far-wake model (NW [9]) and blade element momentum (HBEM [10]). Thereby, the focus lies on comparing QBlade's solvers to their equivalent fidelity counterparts. The results demonstrate the capabilities and limits of lower fidelity aerodynamic solvers and allow a code-to-code comparison between QBlade and HAWC2 on a modern turbine design. Additionally, the baseline rotor of the IEA 10 MW turbine is modified by tip extensions designed within DTU's SmartTip project (Innovation Fund Denmark, 2017-2020). The predicted influence of the tip on aerodynamic loads and aeroelastic interactions provides further distinctions between the different fidelity solvers.

SmartTip Geometries

The SmartTip project focused on the design of innovative blade tip extensions for wind turbines that can be retrofitted to an existing rotor. Their innovative strategy lies within the potential to increase the annual energy production (AEP) up to 6% while allowing to continue with the existing blade structure. Four tip extensions with different geometric properties are simulated in this work. A more detailed description of the SmartTip project is provided in [11, 12, 13, 14]. All tip extensions simulated within the present work are shown in figure 1.

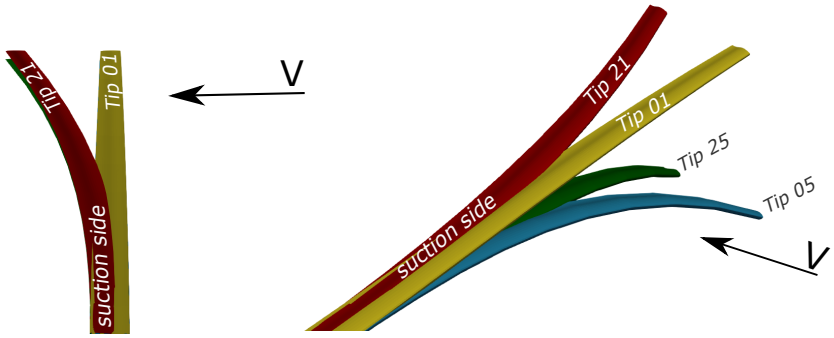

Figure 1. SmartTip extensions, tip 01 - extension, tip 05 - downwind dihedral, tip 21 - backwards sweep and tip 25 - sweep and dihedral

Tip 01 is a blade extension that extends the blade length following the existing curvature. Tip 05 is a downwind dihedral extension, tip 21 a backwards swept extension and tip 25 a combination of the previous two with sweep and dihedral curvature. The respective out-of-plane and in-plane offsets are visible in figure 2. The chord distribution is chosen with the constraint that the chord at the tip of the extension amounts to 50% of the chord at the first inbound section of the tip [14]. Hence, creating different chord distributions depending on the curved length of the extension. All four extensions cause an increase of 5% of the projected radios in an undeflected state.

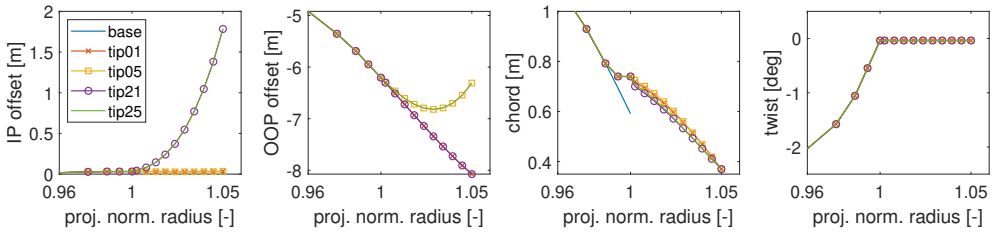

Figure 2. Geometric properties of the SmartTip extensions

2. Numerical Models

The present work represents a study of numerical models of different fidelity levels within the QBlade framework. Each of the models is described briefly in this section. As results of multiple fidelity aerodynamic codes from HAWC2 will serve as comparisons, the underlying algorithms of those particular codes are also briefly introduced. For more details, the reader is referred to the sources within the respective subsections.

2.1. Unsteady Polar-Grid Blade Element Momentum Method

The conventional BEM method is well known and has been described in numerous cases [15, 16], to name a few. The drawbacks of this method, such as an inadequate- or non-representation of radial interaction between the blade sections, out-of-plane effects, shear or skewed inflow require several correction models to make the theory more applicable to real world scenarios. In the following, notable enhancements of the classical BEM method that are implemented into HAWC2 are mentioned. One key innovation to account for azimuthal variations of the induction caused by the azimuthal dependence of blade loadings has been the polar-grid by Madsen et al. [10]. Within it, the annular rings of the BEM approach are divided into stationary azimuthal sub-elements. Each point on the azimuthal grid is associated with a local induction factor, based on the local instantaneous velocity. The latter is approximated by the induced velocity of the neighboring two blades and weighted by their azimuthal distance [10]. Moreover, the calculation point for aerodynamic forces in HAWC2's BEM sits at the three-quarter-chord line [10]. To correct the resulting erroneous lift and drag directions, the pitch rate $\dot{\Theta}$ is used to approximate the angle of attack (AoA) at the quarter-chord line, see [2]. Additionally, the aerodynamic loads of curved blades are multiplied with the correction factor ds/dr to properly reflect the increased curved length in regard to the projected radius of the rotor [10]. The simulations in HBEM were performed with a time step of 0.01 s.

The BEM implementation in QBlade also makes use of the polar-grid to depict local induced velocities more accurately in unsteady conditions. In contrast to HAWC2, the calculation point sits at the quarter-chord position without pitch rate based corrections. As Li et al. state in [2], force directions on dihedral shapes are still modeled correctly, while their magnitude will be erroneous. To correctly model the velocities at curved blade panels, the velocity vectors are projected into their local coordinate system, with the velocity component normal to the section being neglected. The simulations were performed with an aerodynamic time step of 0.05 s.

2.2. Near-Wake

The coupled near- and far-wake model, which is labelled as the near-wake model in the following, may be situated in between the unsteady polar-BEM and the free wake lifting-line methods. In fact, it is a combination of both. The model was first proposed by Beddoes [17] and later introduced in a wind turbine context by Madsen et al. in [18]. Further modifications to the model have been made by Pirrung et al. [19, 20] and Li et al. [9, 21]. The wake is separated into

two regions, the near-wake (quarter rotation of the blade) and the far-wake. In the near-wake region, the induction is calculated through a lifting-line approach, where the induction caused by a vortex element over a quarter of a rotation is approximated by empirical functions. This is more efficient than solving the Biot-Savart law. Since the induction of a quarter rotation of the blade only accounts for part of the total induction, the far wake contribution is computed by a modified BEM model. The sum of both contributions results in the total induction. The near-wake model was further enhanced by the capability to model swept blades by Li et al. [9]. Therefore, the trailing functions described in [19, 20] are extended by a geometrical parameter that allows an analytical treatment of the sweep. To model the bound vorticity on a curved shape, the self-induced velocity is considered [21]. Moreover, to account for out-of-plane shapes of non-planar or deflected rotors, a vortex cylinder model is used [3]. A time step of 0.01 s has been used.

2.3. Lifting-Line Free Vortex Wake

The lifting-line implementation in QBlade largely follows the method that was first laid out by van Garrel in [22] and is detailed in [4]. The blade is modeled by a discretized lifting-line sitting at the quarter-chord point. A bound ring vortex is assigned to each LL element whose circulation can be found by applying the Kutta-Joukowsky theorem:

$$\Gamma = \frac{L}{|v_{tot}|\rho} = C_L(\alpha)\frac{1}{2}|v_{tot}|c. \tag{1}$$

The lift force L is found through the corresponding lift coefficient associated to each aerodynamic section. Γ is the vorticity and ρ the density. The total velocity v_{tot} is calculated through:

$$v_{tot} = v_\infty + v_{mot} + v_\Gamma, \tag{2}$$

with the free stream velocity v_∞, the velocity caused by the motion of the blade v_{mot} and the induced velocity v_Γ that requires the Biot-Savart law to be found. The circulation distribution of the bound vortices is iterated until a distribution that matches the lift and drag coefficients belonging to the actual angle of attack is found. After a convergence state is reached, the blade is advanced in time by one time step and the vortex elements in the free wake are convected with the local velocities [4]. After the wake convection, the bound circulation is shed from the blade to fill up the domain. Thereby, trailing vortices are caused by spanwise gradients and shed vortices by temporal gradients in the circulation [23]. The evaluation point is located at the quarter-chord-point, where the influence of the spanwise bound circulation of the evaluated blade panel is neglected to avoid singularities.

As for the QBEM simulations, the aerodynamic time step was set to 0.05 s. The turbine wake is discretized in four regions with a length of 0.5/2/10 and 20 revolutions respectively. Once a vortex element has reached the end of a region, the streamwise wake lattice resolution is coarsened by a factor of 2. The vortices are modeled with a core radius of 0.05% of the chord lengths and a turbulent vortex viscosity of 796.

2.4. MIRAS

The method for interactive rotor aerodynamic simulations (MIRAS) is a medium fidelity solver with the capabilities to simulate the blade aerodynamics through a viscous-inviscid panel, a potential panel, a lifting surface or a lifting-line method. The presented results in this work were carried out with the latter aerodynamic module combined with a hybrid particle mesh. Similarly to the coupled near- and far-wake model described in section 2.2, the wake is divided into a near- and far-wake region. The blades are modeled as discrete vortex elements which account for the bound vortex strength and release vorticity into the flow (near-wake). In the present method, the

filaments are transformed into vortex particles whose vorticity is interpolated into an auxiliary Cartesian mesh that is used to efficiently calculate their interaction by an FFT-based method (far-wake) [24]. As in the coupled near- and far-wake algorithm, the curved bound vortex self-induction is accounted for with an additional velocity component, see Li et al. [25].
The auxiliary Cartesian mesh employed in all presented cases has a 10Rx4Rx4R expansion, where R is the blade radius of the original geometry. The mesh has a constant spacing of 5 meters in the three directions, adding to a total of more than 1.28 million cells. The bound vortex is discretized with 80 straight segments with a constant spacing, and a time step of 0.04 s has been used.

2.5. EllipSys3D

The CFD results that are referred to as the most accurate physical representation of blade aerodynamics in the present work were computed with the EllipSys3D solver, originally developed at DTU by Sørensen and Michelsen [7, 26, 27]. EllipSys3D is a finite-volume pressure-based incompressible three-dimensional code, that implements several turbulence models. As it was used in this study in the framework of steady simulations, a Reynolds-Averaged Navier-Stokes (RANS) model was selected, and more in particular the k-ω SST [28] implementation. The flow was assumed to be fully turbulent, and a boundary layer clustering was defined in order to resolve the flow around the walls. A structured surface mesh for each of the considered blade geometries was generated, using the openly available Parametric Geometry Library (PGL) tool [29]. A total of 128 cells were used in the spanwise direction, and the chordwise direction was discretized with 256 cells. Inner volume meshes were then generated with the help of the hyperbolic grid generator Hypgrid [30]. A total of 256 cells were used in this process, and the resulting outer domain was located at approximately 11 rotor diameters. The generated volume meshes accounted for a total of 14.2 million cells, and a time step of 0.01 s has been used.

2.6. Aeroelastic coupling

The coupling to the open-source multi-physics engine Project Chrono [31] allows the capability to perform fully aeroelastic simulations in QBlade [4]. The wind turbine model is set up in a multi-body corotational framework and beam elements are modeled by Euler-Bernoulli beams. The structural framework assigns constant parameters along one beam element. The structural model of the IEA 10 MW turbine consists of four bodys, one for each blade and one for the tower. The blades are constrained around the hub node with revolute constraints, allowing for rotations around the pitch axis.
HAWC2 makes use of a multi-body floating reference framework with Timoshenko beam elements instead, allowing for the capability to account for structural shear forces [32]. The turbine is modeled with nine bodies, one for each blade and corresponding hub, one for the tower and tower top and ultimately one for the shaft. Due to the multi body formulation, both tools are capable of simulating nonlinear behaviour. A difference between both structural formulations is that HAWC2 allows for a gradient in the structural properties along one beam element.

3. IEA 10 MW Turbine

The simulations were performed on a preliminary model of the IEA 10 MW turbine that slightly deviates from the official release of the IEA report [33]. This reference turbine is representative for modern offshore turbine designs. The affiliated turbine class is 1A. Furthermore, it has a rotor diameter of 198 m, a hub height of 119 m and the rated power is reached at 10 MW. In order to allow for a fair comparison, the model set up in QBlade intents to replicate the one from HAWC2 as close as possible. A hub diameter of 5.6 m was used. Precone and tilt angles were set to zero degrees. The blade is discretized with 50 aerodynamic sections with a finer resolution in the root and tip regions. The structure of one blade is represented by 19

structural nodes along the span (both distributions match exactly with the HAWC2 model). The aerodynamic characteristic is given by the FFA-W3 airfoil family. The polars were computed with the 2D CFD solver EllipSys2D [7] assuming a fully turbulent boundary layer at a Reynolds number of Re = $1 \cdot 10^7$ without 3D corrections. The tool AirfoilPrep.py [34] was used for the 360° extrapolation. This data was shared by the DTU Wind Energy Group. Since the blade transitions smoothly from thick circular profiles at the root to the thin profiles at the blade tip, the polars were interpolated with the thickness serving as the defining parameter. The tip extensions are discretized with ten additional aerodynamic sections and 20 beam elements, resulting in a total of 60 aerodynamic sections and 39 beam elements for each blade that includes a tip extension. The tower structure is discretized with eleven nodes in QBlade and 20 nodes in HAWC2, the additional nodes being by virtue of the continuous assignment of structural properties to model steep gradients in between two tower sections.

4. Simulation and Results

This section shows results from two load cases. The first case is an idealized power curve with prescribed rotational speed (rpm), pitch angle and uniform inflow conditions. The second load case resembles the first one but includes structural dynamics and the DTU Wind Energy Controller [35] for power regulation. Both cases include the baseline rotor and the four extended SmartTip rotors.

4.1. Rigid Aerodynamic Simulations

Figure 3 shows the relative difference in aerodynamic power and thrust of the compared methods in relation to the CFD solution over the full operating range of the turbine. In the power difference, QBlade's BEM, its lifting-line, the HAWC2 BEM and the near-wake code demonstrate similar characteristics. At cut-in wind speed, their respective difference amounts to the maximum and converges to the CFD result at and above rated wind speed (11 ms^{-1}). The cause for this converging behaviour may be explained by the reduction of the axial induction factors with increasing wind speed [36]. The influence of the wake modeling approach on blade loading therefore reduces with increasing wind velocities. In these high tip-speed-ratio conditions, both BEM codes fail to resemble the solution of the higher fidelity methods with deviations of 18% (HBEM) and 23% (QBEM) respectively. From all codes, MIRAS matches the CFD curve the best, closely followed by the QBlade lifting-line curve. The thrust difference shows a similar pattern between the four codes as well. Their relative difference again converges to the CFD result from cut-in to rated wind speed. Unlike in power, a slight divergence tending towards an overprediction of thrust above rated conditions is visible. The smaller relative differences compared to power are caused by the larger magnitude of the out-of-plane forces than the ones acting in in-plane direction. This is especially pronounced at low wind speeds.

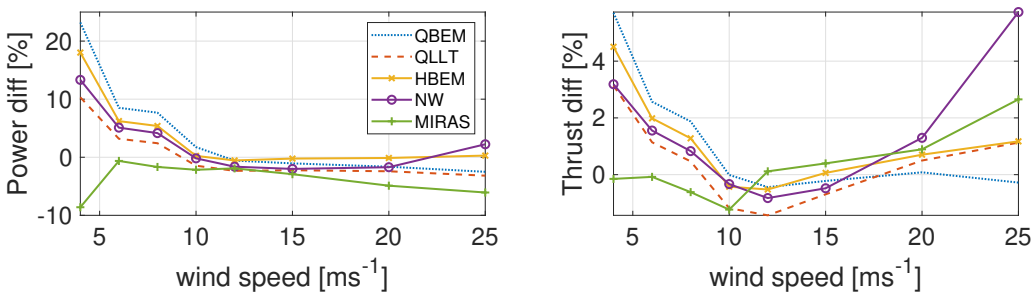

Figure 3. Relative power and thrust difference in reference to the CFD power curve

In order to better understand the cause for the differences in the rotor torque and power, figure 4 depicts the load distributions over the span of the blade at 6 ms^{-1} and 8 ms^{-1} wind speed. The loads in both directions display generally good agreement in the mid span region to the CFD results. Deviations are most pronounced in the vicinity of the root but also the tip regions and may be accounted to the use of 2D polar data in all codes except CFD. This observation was made in [21, 19] and since both QBlade codes also rely on the airfoil polars to model aerodynamic forces, they demonstrate a similar pattern. More precisely, the out-of-plane loads are overpredicted by both BEM codes and, to a lesser degree, of the near-wake code across the sections at 85% of the projected radius. In the more inbound regions, good agreement between all compared codes is visible. The load distributions in in-plane direction demonstrate similar trends with regard to the difference at the root region. However, a more notable difference between the fidelity groups is visible. While the QLLT curve almost coincides with the CFD distribution in the tip region, a slight underprediction by MIRAS is visible. The difference in this area of the blade, which is critical for power generation, is expressed in the relative power difference in figure 3 at the corresponding wind speeds. The lower fidelity BEM codes overpredict the in-plane forces in the outer third of the radius considerably, thus explaining the overprediciton in power. The near-wake curve, being the code that combines both aerodynamic approaches, behaves closer to the lifting-line curves around 85% of the radius and closer to the BEM curves near the vicinity of the tip.

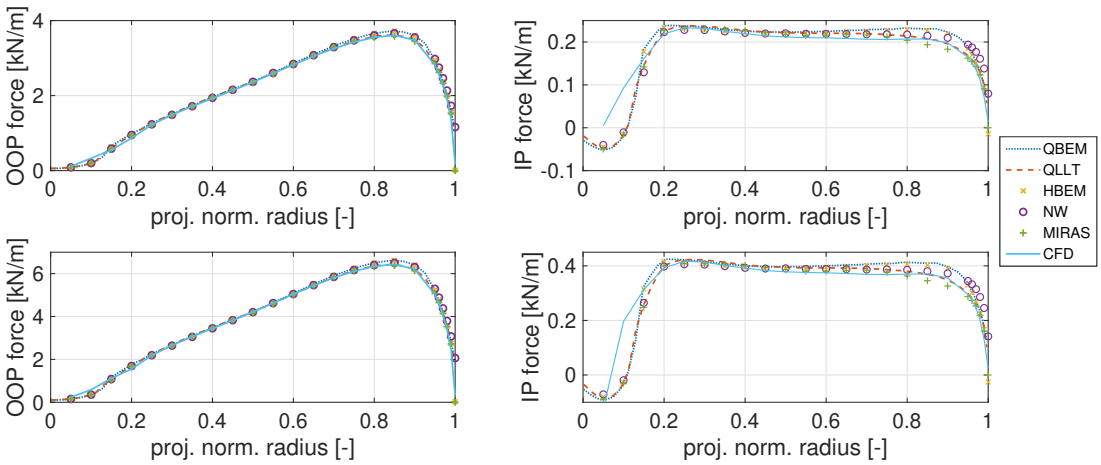

Figure 4. Distributed loads on the baseline rotor at 6 ms^{-1} (top) and 8 ms^{-1} (bottom) wind speed

To evaluate the accuracy in the prediction of aerodynamic loads along strongly curved tip regions, the in-plane and out-of-plane loads are analyzed in figure 5, specifically along the span of the tip extensions. Here, all compared codes agree in the solution with a decrease of the loads along the span in both directions. The remaining extensions are presented in form of their difference to the loads at tip 01, each code subtracted by its respective solution to depict the predicted influence of the curvature. QBlade's lifting-line agrees with the CFD curve regarding the major patterns due to the influence of the dihedral (tip 05) and swept (tip 21) shapes as well as of the combination of both (tip 25). It qualitatively shows a close accordance to MIRAS in the out-of-plane loads and in-plane loads. Both BEM codes demonstrate a similar behaviour to each other for all tip shapes. The influence of the dihedral angle is represented well. As soon as a sweep angle is included in the geometry, both fail to predict the increase in loads when the radius is close to the vicinity of the tip. This sudden increase of the tip loads in the higher

fidelity methods may be explained with two phenomena. First, the sweep causes a projection of the velocity perpendicular to the section resulting in a reduced effective velocity and hence a higher angle of attack. The second phenomenon was analyzed by Riziotis et al. [37], where he states that the vorticity of (backwards) swept sections is shed further downstream compared to the more inboard sections, resulting in a local decrease of the induced velocity at the vicinity of the tip and thus an increase of the local AoA. The latter effect can't be captured by the BEM approach due to the assumption that aerodynamic sections do not interact with their adjacent neighbors [37].

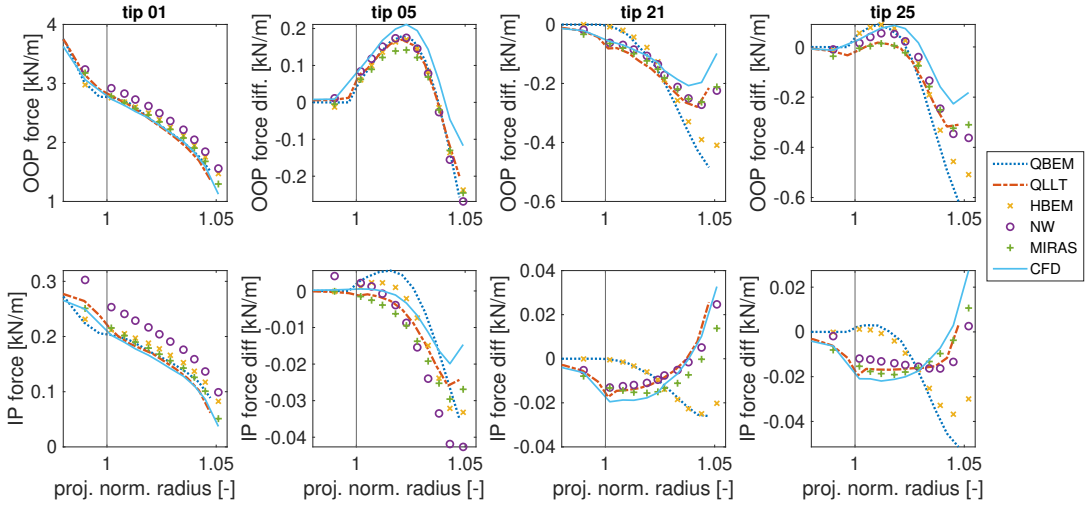

Figure 5. Distributed in- and out-of-plane loads along tip 01 and the difference in loads to tip 01 at 8 ms^{-1} wind speed. The vertical line marks the beginning of the extension

To analyze the influence caused by the SmartTip geometries on an integral level of each computational method, figure 6 demonstrates the influence of the respective tip extension in relation to the corresponding CFD result at the representative wind speed of 8 ms^{-1}. For the rigid aerodynamic simulations, an almost constant behaviour of all codes is evident. The difference to the CFD results may be ordered by fidelity, where both BEM methods show the largest offsets. The near-wake code yet again demonstrates that it can bridge the fidelity gap and lies in between the lower fidelity BEM results and both lifting-line based solvers. A similar pattern can be seen in the thrust however, with considerably smaller relative differences to CFD.

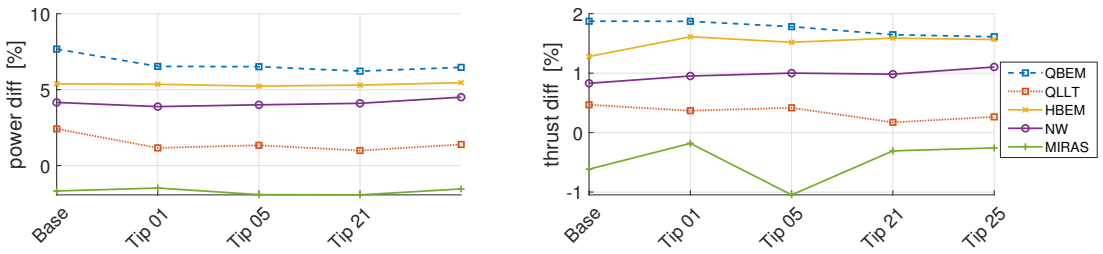

Figure 6. Influence of the SmartTip extension on the aerodyn. power and thrust in reference to the corresponding CFD solution at 8 ms^{-1} wind speed

4.2. Aeroelastic Simulations

The modeling of the coupled aero-elastic wind turbine dynamics adds considerable complexity to the simulation since any deformation directly influences the aerodynamic forces and vice versa. Furthermore, power regulation is handled by a controller, introducing the need to consider inertial and control forces. In this section, first the power and thrust of the baseline rotor will be shown. Second, key parameters such as root bending moments (RBMs) and tip deflections are displayed over the azimuthal position for the baseline and swept rotors, since the aerodynamic loads on the backwards sweep suggest the largest discrepancies. Apart from the CFD solver, the same aerodynamic codes of the HAWC2 tool serve as comparisons. Figure 7 illustrates the aerodynamic rotor power and torque. Few deviations regarding both integral values below rated wind speed can be determined, the strongest being visible at 10 ms^{-1}. Hence, this operation point is chosen for a further, more detailed comparison of the codes in the time domain.

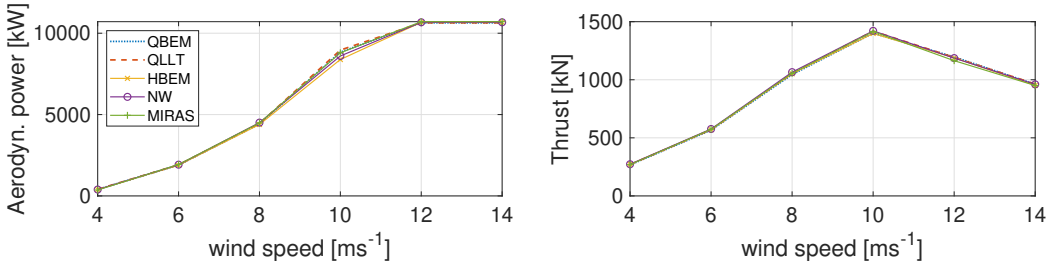

Figure 7. Aerodyn. power and thrust of the baseline rotor, aeroelastic load case

Figures 8 and 9 show the root bending moments[1] and tip deflections of the baseline and swept rotors. The parameters are presented over one complete rotation of a blade after a converged state was reached. For the baseline rotor, the out-of-plane RBMs demonstrate good agreement between all compared codes regarding their phase angles. Differences in the magnitude of the mean value around which the moments oscillate are present. Thereby, QBEM underestimates the out-of-plane RBM in comparsion to QLLT regarding the mean. Moreover, the amplitude of the lower fidelity code shows an increased amplitude throughout the oscillation in comparison to the QLLT result. Compared to their similar fidelity counterparts, QLLT shows a higher mean value but smaller amplitude than MIRAS. The QBEM curve also predicts higher out-of plane RBMs compared to HBEM, demonstrating a closer result to the medium fidelity codes. In the in-plane direction, the results are closely matched with slightly larger amplitudes in both QBlade results. In the torsional degree of freedom (DOF), no differences in the phase angles are visible. Yet, the mean value of the oscillation from both QBlade results is slightly shifted towards lower torsional moments. The swept tip influences the previous observations mainly in the out-of-plane RBM. The increase of the RBM caused by the extension is more pronounced in the three HAWC2 codes e.g., the MIRAS curve now displays a similar mean value compared to QLLT. This effect is also true for the QBEM curve, where lesser increase in the RBM compared to HBEM is estimated. More pronounced however, is the now existing difference in the phase angle that is present between QBEM and, to a lesser degree, QLLT compared to the HAWC2 solutions. While the HAWC2 curves show almost no difference in the phase compared to the baseline, both QBlade curves are shifted towards smaller angles.

Figure 9 shows the tip deflection in the out-of-plane and in-plane directions. The out-of-plane deflection demonstrates very close agreement between QBlade's LL and BEM curves. Both agree well regarding the phase angle with MIRAS and the NW code, with offsets of approximately 0.2 m in between them. Similarly to both fidelity solvers from QBlade, HBEM and MIRAS agree

[1] The moments are computed around radius 2.89 m (closest position to the root where HAWC2 data is available)

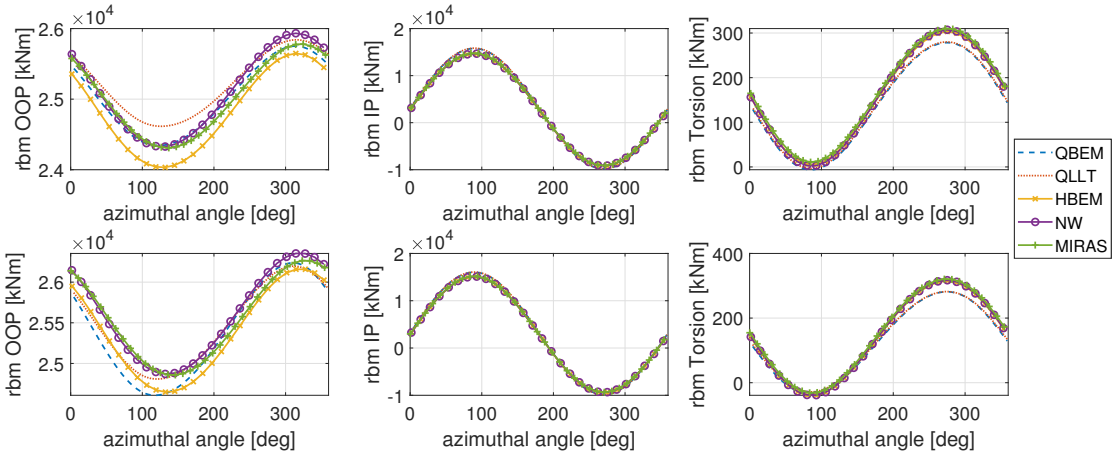

Figure 8. Root bending moments (at r = 2.89 m) in the out-of-plane, in-plane and torsional DOF at 10 ms^{-1} wind speed. Baseline (top), swept rotor (bottom)

well in the mean out-of-plane tip deflection but show larger discrepancies in the phase angle. In tangential direction, practically no differences are present. The swept tip causes a larger tip deflection in all three HAWC2 codes regardless of the aerodynamic fidelity. This very detailed comparison shown in figures 8 and 9 indicates that the distinctions in the structural modeling between QBlade and HAWC2 outweigh the differences in accuracy between the medium and low fidelity aerodynamic models.

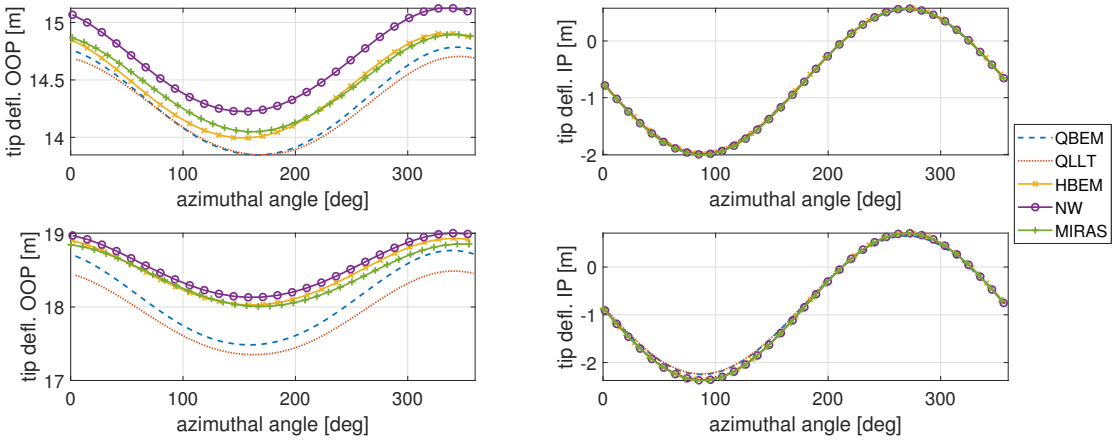

Figure 9. Tip deflections in out-of-plane and in-plane direction at 10 ms^{-1} wind speed. Baseline (top), swept rotor (bottom)

5. Conclusion

In this work a comparative study between a low fidelity BEM and medium fidelity LL code within the simulation tool QBlade is presented. Two load cases with differing complexity were considered to provide a holistic assessment of the capabilities of the codes. Multiple fidelity simulations carried out by the DTU Wind Energy Group in the simulation tool HAWC2 were

steadily referred to as references.
Results of purely aerodynamic simulations imply the strongest deviation from the CFD code in high tip-speed-ratio scenarios. Thereby, with increasing fidelities, smaller deviations from the CFD result were present. On an integral level, QBlade's BEM code was found to perform similarly to the one of HAWC2. In regards to load distribution in tangential and normal direction both continued do demonstrate similar results on the baseline rotors, overpredicting the loads along the outer radius. The load distribution along the strongly curved tip extensions revealed difficulties in the BEM code to reflect the increase in loads at the vicinity of the swept tip extension. A failure to accurately simulate the induced velocity and subsequently the correct angle of attack is presumably the cause for this. Again, this was in accordance with the results of the HAWC2 BEM. The increased fidelity level of the lifting-line solver implemented in QBlade improved the accuracy with regard to the CFD results, both on an integral level but also considering the load distribution along the baseline blade. The loads along the curved tip extensions were largely accurate and showed comparable offsets to the CFD solution as the other medium fidelity codes MIRAS and NW. Interestingly, the offsets to CFD on an integral level were not significantly influenced regardless of the curvature of the tip extension.
When the structural dynamics were accounted for in aeroelastic simulations, the direct comparison became more vague as additional uncertainties between the two simulation frameworks were introduced. Nevertheless, good agreement between both simulation tools were found. More specifically, the results within a simulation framework seemed to align better notwithstanding the fidelity level of the aerodynamic model. For the baseline rotor, key parameters such as RBMs and tip deflections showed similar results regarding mean values as well as phase and amplitude over a full rotation, with slightly smaller out-of plane tip deflections in both QBlade results. Moreover, the influence of the swept tip extension resulted in a lesser increase in the out-of plane tip deflection compared to HAWC2 and a phase shift in the out-of-plane RBM that was especially pronounced in the QBEM result.
Whether the increased importance of the structural model compared to the aerodynamic fidelity when modern turbine designs are simulated can be confirmed in dynamic load cases as well, could be part of future work. Furthermore, a detailed comparison of only the structural models could potentially decrease the level of uncertainty in such a steady load case comparison and help to better understand the increasing discrepancies between aerodynamic codes of similar fidelity when structural dynamics are accounted for.

References

[1] Veers P et al. 2019 Grand challenges in the science of wind energy *Science* **366** eaau2027 `https://science.org/doi/10.1126/science.aau2027`
[2] Li A, Gaunaa M, Pirrung GR, Forsting AM and Horcas SG 2022 How should the lift and drag forces be calculated from 2-D airfoil data for dihedral or coned wind turbine blades? *Wind Energ. Sci. Discussions* [preprint] in review `https://doi.org/10.5194/wes-2021-163`
[3] Li A, Gaunaa M, Pirrung GR and Horcas SG 2022 A computationally efficient engineering aerodynamic model for non-planar wind turbine rotors *Wind Energ. Sci.* **7** 75–104
[4] Marten D 2020 *QBlade: A Modern Tool for the Aeroelastic Simulation of Wind Turbines* PhD thesis Technische Universität Berlin, Berlin
[5] Marten D, Saverin J, Behrens de Luna R and Perez-Becker S *QBlade Documentation* `https://docs.qblade.org/`
[6] Larsen TJ and Hansen AM 2019 *How 2 HAWC2, the User's Manual* Manual Forskningscenter Risø-R-1597, Roskilde
[7] Sørensen NN 1995 *Block General Purpose Flow Solver Applied to Flow Over Hills* PhD thesis Risø National Laboratory, Roskilde
[8] Ramos-García N, Sessarego M and Horcas SG 2021 Aero-hydro-servo-elastic coupling of a multi-body finite-element solver and a multi-fidelity vortex method *Wind Energ.* **24** 481-501
[9] Li A, Pirrung GR, Gaunaa M, Madsen HA and Horcas SG 2022 A computationally efficient engineering aerodynamic model for swept wind turbine blades *Wind Energ. Sci.* **7** 129–160

[10] Madsen HA, Larsen TJ, Pirrung GR, Li A and Zahle F 2020 Implementation of the blade element momentum model on a polar grid and its aeroelastic load impact *Wind Energ. Sci.* **5** 1-27
[11] Barlas T, Pirrung G, Ramos-García N, Horcas SG, Mikkelsen RF, Olsen AS and Gaunaa M 2021 Wind tunnel testing of a swept tip shape and comparison with multi-fidelity aerodynamic simulations *Wind Energ. Sci.* **6** 1311-1324
[12] Barlas T, Ramos-García N, Pirrung GR, Horcas SG 2021 Surrogate-based aeroelastic design optimization of tip extensions on a modern 10 mw wind turbine *Wind Energ. Sci.* **6** 491-504
[13] Zahle F, Sørensen NN, McWilliam MK and Barlas A 2018 Computational fluid dynamics-based surrogate optimization of a wind turbine blade tip extension for maximising energy production *J. Phys.: Conf. Ser.* **1037** 042013
[14] Horcas SG, Barlas T, Zahle F and Sørensen NN 2020 Vortex induced vibrations of wind turbine blades: influence of the tip geometry *Phys. Fluids* **32** 065104
[15] Hansen OL 2008 *Aerodynamics of Wind Turbines* vol 2 (London, Earthscan) pp 45-52
[16] Burton T, Sharpe D, Jenkins N and Bossanyi E 2001 *Wind Energy Handbook* (John Wiley & Sons, West Sussex) pp 59-68
[17] Beddoes TS 1987 A near wake dynamic model *Aerodynamics and Aeroacoustics National Specialist Meeting Papers and Discussion* p 1-9
[18] Madsen HA and Rasmussen F 2004 A near wake model for trailing vorticity compared with the blade element momentum theory *Wind Energ.* **7** 325-341
[19] Pirrung GR, Madsen HA, Kim T and Heinz J 2016 A coupled near and far wake model for wind turbine aerodynamics *Wind Energ.* **19** 2053-2069
[20] Pirrung GR, Riziotis V, Madsen HA, Hansen M and Kim T 2017 Comparison of a coupled near- and far-wake model with a free-wake vortex code *Wind Energ. Sci.* **2** 15-33
[21] Li A, Pirrung G, Madsen HA, Gaunaa M and Zahle F 2018 Fast trailed and bound vorticity modeling of swept wind turbine blades *J. Phys.: Conf. Ser.* **1037** 062012
[22] van Garrel A 2003 *Development of a Wind Turbine Aerodynamics Simulation Module* Techn.Rep:. ECN-C–03-079 Energy research Centre of the Netherlands, Netherlands
[23] Perez-Becker S, Papi F, Saverin J, Marten D, Bianchini A and Paschereit CO 2020 Is the blade element momentum theory overestimating wind turbine loads? – An aeroelastic comparison between openfast's aerodyn and qblade's lifting-line free vortex wake method *Wind Energ. Sci.* **5** 721–743
[24] Ramos-García N, Hejlesen MM, Søensen JN and Walther JH 2017 Hybrid vortex simulations of wind turbines using a three-dimensional viscous-inviscid panel method *Wind Energ.* **20** 1871-1889
[25] Li A, Gaunaa M, Pirrung GR, Ramos-García N and Horcas SG 2020 The influence of the bound vortex on the aerodynamics of curved wind turbine blades *J. Phys.: Conf. Ser.* **1618** 052038
[26] Michelsen JA 1992 *Basis3D-a Platform for Development of Multiblock PDE Solvers* Techn. Rep.: AFM 92-05 Technical University of Denmark, Denmark
[27] Michelsen JA 1994 *Block Structured Multigrid Solution of 2D and 3D Elliptic PDE's* Techn. Rep.: AFM 94-06 Technical University of Denmark, Denmark
[28] Menter F 1994 Two-equation eddy-viscosity turbulence models for engineering applications *AIAA Journal* **32** 1598-1605
[29] Zahle F 2019 *Parametric Geometry Library (PGL)* `https://gitlab.windenergy.dtu.dk/frza/PGL`
[30] Sørensen N 1998 *Hypgrid2D a 2-D Mesh Generator* Techn. Rep.: RISO-R-1035(EN) Risø National Laboratory, Denmark
[31] Tasora A et al. 2016 *Chrono: An Open Source Multi-Physics Dynamics Engine* In Proc. of HPCSE Conf, Solán
[32] Gözcü O and Verelst DR 2020 The effects of blade structural model fidelity on wind turbine load analysis and computation time *Wind Energ. Sci.* **5** 503-517
[33] Bortolotti P, Tarrés HC, Dykes K, Merz , Sethuraman L, Verelst D and Zahle F 2019 *IEA Wind TCP Task 37: Systems Engineering in Wind Energy - WP2.1 Reference Wind Turbines* Techn. Rep.: NREL/TP-5000-73492 US
[34] Ning SA 2013 *Airfoilprep.py Documentation* Techn. Rep.: NREL/TP-5000-58817, US
[35] Hansen MH, Henriksen LC 2013 *Basic DTU Wind Energy Controller* Techn. Rep.: 0028 DTU Wind Energy, Denmark
[36] Jeong M, Kim S, Lee I and Yoo S 2014 Wake impacts on aerodynamic and aeroelastic behaviours of a horizontal axis wind turbine blade for sheared and turbulent flow conditions *Journal Of Fluids And Structures* **50** 66-78
[37] Riziotis V, Manolas D and Voutsinas S 2011 *Advanced Aeroelastic Modelling of Swept Rotor Blades* In Proc. of EWEA Conf., Brussles